Hyperspectral Image Unmixing for Land Cover Classification

Amol D. Vibhute*[1]
School of Computer Science, MIT-World Peace University,
Pune (411038), MH, India.
amolvibhute2011@gmail.com

Sandeep V. Gaikwad, Karbhari V. Kale
Dept. of Computer Science & IT, Dr. BAM University,
Aurangabad (431004), MH, India.
sandeep.gaikwad22@gmail.com, kvkale91@gmail.com

Arjun V. Mane
Dept. of Digital & Cyber Forensic, Government Institute of Forensic Science,
Nagpur, MH, India.
arjunmane7113@gmail.com

***Abstract*— Hyperspectral image unmixing is a very essential but challenging task for solving the mixed pixel issues. Spectral unmixing is directly involved in image sub-pixel classification, answering the spectral mixing problem. The present study emphasizes the importance of unmixing spectral features from remotely sensed hyperspectral scenes to classify land features. The high spectral and moderate spatial resolution Jupiter Ridge AVIRIS hyperspectral image was used to test the endmember, unmixing and classification algorithms. The study has been done by atmospheric correction, dimensionality reduction, endmember extraction, spectral unmixing, and classification. The results show that the implemented methodology has provided four endmembers to unmix the image and abundances maps and Spectral Angle Mapper (SAM) based classification with 94.19% accuracy. It was shown that improved unmixing methods are vital to tackle spectral variability to obtain accurate abundances estimations. The present research can be helpful in the development of new unmixing algorithms.**

Keywords*— *Hyperspectral unmixing, Sub-pixel classification, endmember extraction, MNF, Spectral angle mapper.

I. INTRODUCTION

Hyperspectral remote sensing sensor captures a 3-D view cube developed through hundreds of narrow and constant channels containing the electromagnetic spectrum, delivering meaningful image information. The pixel spectra may be mixed with other numerous elements caused by the hyperspectral sensors low spatial resolution, several scattering effects, and other microscopic material mixing, resulting in lots of mixed pixels [1], [2]. Consequently, unmixing mixed pixels from remotely sensed hyperspectral images is essential for processing the hyperspectral image [2], [3]. Hyperspectral Unmixing (HSU) assesses the quantities of component items of a combined pixel. However, the spectrally matched picture elements can be estimated via the linear mixing model [3]. HSU is a procedure to detect the "pure" spectral signatures of objects frequently referred to as an endmember. In addition, HSU estimates endmembers' respective proportions, namely the abundance fractions to the measured spectra at each pixel. The purpose of HSU is to extract the endmembers (pure pixels) from the mixed pixels and to determine their respective abundances [2], [3], [4], [5]. HSU has many uses such as mapping of sub-pixels [6], [7], enhancing hyperspectral images [8], high-resolution hyperspectral imaging [9], hyperspectral image compression and its reconstruction [10], crop classification [5], target detection [11], wild animal tracking [5], etc.

However, the sub-pixel classification is complicated and cannot be correctly classified by conventional brutal methods [7]. HSU is an efficient measure to solve the issue of mixed pixels. Therefore, sub-pixel hyperspectral image classification is possible to complete using the computation of HSU. Several studies have been done on the HSU for hyperspectral image classification. For instance, an author's [5] has used artificial neural networks based on a hybrid (linear and nonlinear) approach to unmix the hyperspectral data. The study [12] assessed the pure pixels quality, quantity, and performance of spectral unmixing models using a hyperspectral image.

Similarly, the study [7] uses hyperspectral images to solve the mixed pixel problem proposing MBQPSO (modified binary quantum particle swarm optimization) subpixel mapping method. In the study [13], authors have extracted endmembers in AVIRIS hyperspectral image using two spectral unmixing techniques to classify the land features. In [3] study, a new unmixing method was proposed to discover an original hyperspectral image's subspace arrangement and integrate it into the limited non-negative matrix factorization (NMF) framework to promote unmixing performance. However, the study [4] has improved the classification accuracy based on the abundance-based multi-hyperspectral image classification method. The study has [4] used a neural network approach to enhance the hyperspectral image classification performance with a spectral unmixing method.

However, the researchers have proposed several methods to unmix the mixed pixels from hyperspectral and multispectral images. As far as this, spectral unmixing has been widely used for classifying the spectral signatures of land patterns at a single time point. The acquired spectral information is inadequate for each time frame of the image. It is difficult to estimate the end members accurately through insufficient spectral information. Therefore, spectral unmixing of remotely sensed pictures is still challenging due to the availability of various ground features. The spectral signatures in a remote sensing image may be similar due to these ground components and low spectral resolution images [14].

Therefore, the present work emphasizes spectral unmixing of remotely sensed hyperspectral images for sub-pixel classification of land cover features. The content of this manuscript is separated into four sections. This section briefly describes the present study, related literature, and the challenges in unmixing remote sensing images. Used hyperspectral datasets for the present study and implemented methodology has been given in section second. A detailed discussion of results is given in section three. This portion also highlights the results, accuracy assessments, and generated classification map of the land cover patterns. Section four concludes the present study.

II. MATERIALS AND METHODS

A. Hyperspectral Data

These paper experiments were done on the widely used Jasper Ridge [15] hyperspectral image depicted in Fig. 1. The Jasper Ridge image is acquired by the Jet Propulsion

2021 IEEE India Council International Subsections Conference (INDISCON) | 978-1-6654-3833-9/21/$31.00 ©2021 IEEE | DOI: 10.1109/INDISCON53343.2021.9582217

Laboratory (JPL) using the Airborne Visible/Infrared Imaging Spectrometer (AVIRIS) sensor [2]. The spatial resolution of the Jasper Ridge image is about 20 meters [2]. The original Jasper Ridge image consists of 512 x 614 pixels. Every pixel is captured at 224 spectral bands extending from 380 to 2500nm with high spectral resolution up to 9.46nm [15].

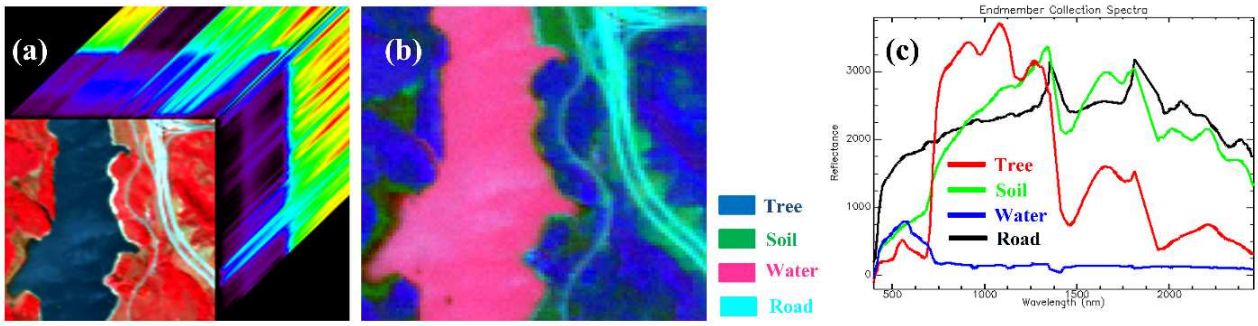

Fig. 1. (a) the illustration of a false colour composite of the Jasper Ridge hyperspectral scene, (b) ground truth abundances scene, (c) ground truth endmembers.

B. The Methodology

1) Pre-processing

Since the original Jasper Ridge hyperspectral scene is exceptionally complicated to acquire the ground truth, therefore, the subset of 100 x 100 pixels was computed [15]. However, the initial pixel begins from the (105, 269)-th pixels [15]. The remote sensing images contain lots of noise due to atmospheric effects and dense water vapor. The provider atmospherically corrected the obtained Jasper Ridge hyperspectral image. Therefore, the hyperspectral image (Fig. 1) used in this research has already converted from radiance to reflectance. However, much extra information captured by the sensors does not add to the essential information for a specific application. There is frequently overlap of significant information over the bands of image for a given pixel. Consequently, feature selection and unwanted bands reduction are vital to hyperspectral image analysis [16]. These unwanted bands were subset to out for spectral reduction. The spectral channels 1-3, 108-112, 154-166 and 220-224 were eliminated, and the remaining 198 channels were used for further processing [2], [15], [17]. Eliminating the noisy channels, the hyperspectral image size is 100 x 100-pixel x 198 bands for height, width, and depth, respectively. The remaining processing has been done on the converted image.

2) Dimensionality Reduction and Noise Segregation

Hyperspectral image bands are often correlated, and some of them contain slight noise even after unwanted bands removal. Hughes phenomenon says, more bands create inaccurate results or less accuracy [18]. In addition, the analysis of all original spectral bands is ineffective and leads to inaccurate results. Moreover, the Least-Squares Linear unmixing (LSLU) approach [13] is sensitive to hyperspectral image noise. Thus, the elimination of redundant bands and noise segregation is essential to avoid such issues. In the present study, the maximum noise fraction (MNF) transformation [19], [20] method has been used to reduce the spectral dimensions, to segregate the noise in the scene, to generate the quality components, and reduce the computational constraints for further processing. After the MNF transformation, the image data have assessed by the large, correlated eigenvalues and consistent eigen images. However, the irrelevant eigenvalues were also obtained with images that contain noise. The eigenvalues for the bands that cover information are ordered at the higher level. The consistent eigenvalues are noise removed, and dimensionality diminished images. The plot of MNF eigenvalues is shown in Fig. 2, which defines the break-in eigenvalues slope and MNF cut-off between noise and signals. In this study, high eigenvalues bands were chosen to reduce the spectral dimension from 198 to 20.

3) Spectral Unmixing

a) Linear mixing model (LMM)

An LLM model applied in the current paper is suitable for defining hyperspectral images when the image's descent and the remote connections between the detected objects are insignificant. The linear amalgamation of reflected spectra of an image feature in the pixel with known pure pixels is used to model any channel's noted pixel value. The pure object spectra are provided using this model [13], [14]. The LM model can be mathematically written as (Eq. 1),

$$A_i = \sum_{j=1}^{n} M_{ij} R_j + E_i \quad (1)$$

Where, i=1,..,b (bands number), j=1,…..,s (pure spectra's number), A_i=spectral reflectance of the ith spectral band of a pixel, Mij=jth objects known spectral reflectance, Rj=the fraction coefficient of the jth object within the pixel, Ei= represents an additive noise for the ith spectral band [13].

The pure pixels can be used to accomplish a practical endmember estimation. Therefore, it is essential to use the critical abundance information for getting pure pixels. It will be helpful in the precise estimation of end members to enhance the abundance estimation accuracy. Thus, spectral unmixing is an optimization problem that is resolved using frequently rotating the estimation between the endmember update and the abundance estimation [13], [14].

b) Least-Squares (LS) Linear Unmixing

The abundances can be estimated using LS unmixing solution when the endmember numbers and their spectral signatures are known. In LS unmixing, while reducing the errors sum square, the unmixing coefficients can be obtained. When the two abundance constraints are disregarded, then the pixel restoration error is minimized [13]. The LS can be solved using Equation (2) [13],

$$\hat{R} = (M^T M)^{-1} M^T A \quad (2)$$

4) Classification based on Spectral Angle Mapper (SAM)

In the present study, the SAM method is implemented, which is based on spectral classification methods. The SAM method uses the n-D angle of the hyperspectral image to match the pure pixels (endmembers) to the reference spectra or spectral library while determining the spectral similarity between the two spectra. This method calculates

hyperspectral image pixels and estimates the relevant spectra. The input is endmember spectra for the SAM method, obtained through the spectral library, pure spectral or extracted spectra by ROIs. Mathematically SAM method is calculated using Eq. 3 [21].

$$\alpha = \cos^{-1}\left(\frac{\sum_{i=1}^{nb} t_i r_i}{\left(\sum_{i=1}^{nb} t^2{}_i\right)^{1/2} \left(\sum_{i=1}^{nb} r^2{}_i\right)^{1/2}} \right) \quad (3)$$

where, t stands for the test spectra, r stands for the reference spectra and $_{nb}$ stands for the channels number. More theory illustrating the angle between the reference spectrum and test spectrum will be found at the reference in detail [21].

III. Results and Discussions

The downloaded Jasper Ridge hyperspectral image in this experiment was used to test the unmixing and classification algorithms. The provider has done the atmospheric correction on the original datasets. In addition, unwanted and water vapor channels were eliminated from the original data for the remaining work. Thus, the image with 100x100 pixels and198 spectral bands were used to test the experiments.

A. MNF Transformation

The MNF transformation [19], [20] algorithm has been implemented to segregate the noise and extract the most relevant bands from the original image. The noise statistics were assessed from the original image for the transformation. After the MNF transformation, the original image has generated new bands. The eigenvalues were used to determine and denote the dimensionality of the image pixels. It has observed by the eigenvalues image, and the first 20 bands were reached the maximum eigenvalues (Fig. 2) among the 198 bands. Thus, only the first 20 bands were selected as a new set of 20 MNF bands and used to input spectral unmixing. The remaining bands were ignored from further processing due to higher noises. The cut-off number is decided by verifying the MNF eigenvalue plot demonstrated in Fig. 2.

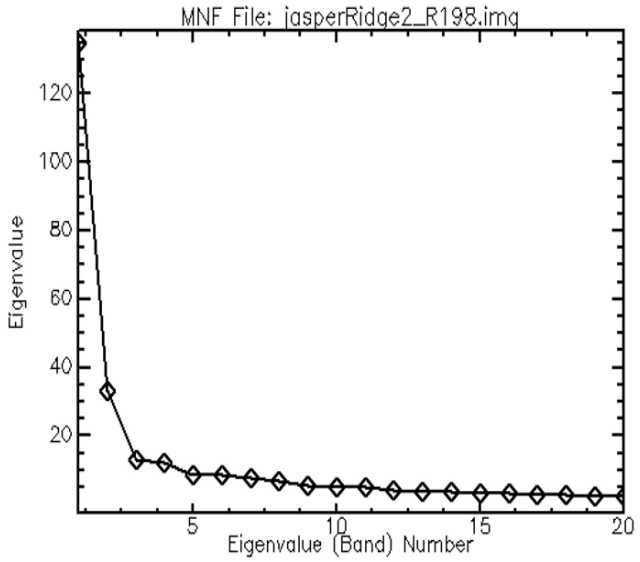

Fig. 2. The MNF eigen value plot.

B. Hyperspectral Image Unmixing

Firstly, the hyperspectral image unmixing process has been performed on 20 MNF transferred bands extracted from the original image. The class abundance maps resulted from LS unmixing are depicted in Fig. 3. The class-specific abundance images (Fig. 3) show the outcomes of sub-pixel classification. However, they do not directly demonstrate the distribution of classified regions. The abundance image's primary (brighter) pixel value (Fig. 3) identifies the endmembers and maps the particular class for classification output. In our case, four endmembers were identified, such as (1) Tree, (2) Soil, (3) Water and (4) Road (Fig. 4) after correction of Jasper Ridge hyperspectral image [2], [15], [17]. As shown in Fig. 4, the pure pixels (endmembers) are labeled with four land cover classes.

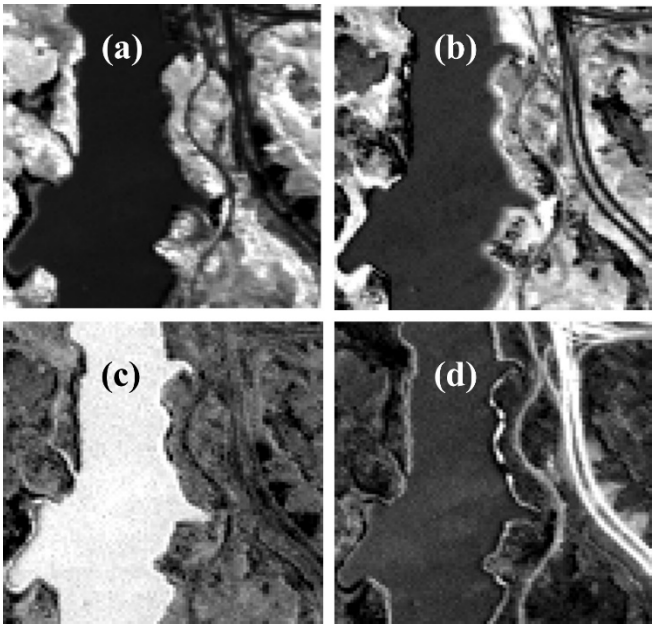

Fig. 3. The class abundance maps (a) Tree, (b) Soil, (c) Water, and (d) Road respectively resulted from LS unmixing.

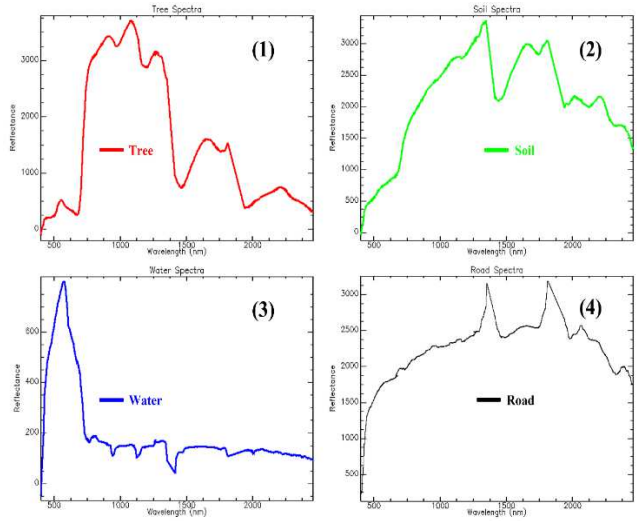

Fig. 4. Four endmembers (1) Tree, (2) Soil, (3) Water, and (4) Road, correspondingly.

C. Classification and Accuracy Assessment

Spectral unmixing does not provide any label directly to any pixels. Thus, the pixel-based SAM method has been used

to classify the mixed pixels with a specific class label. The abundance maps were given input to the SAM method, and a thematic map (Fig. 5) was generated. The largest (brighter) pixel value in the abundance image (Fig. 3) has been applied to train the SAM classifier and test the classified image. The classified map (Fig. 5) was used to assess the accuracy. However, the unmixing results lead to some failure of information and accuracy. Nonetheless, this is one of the common approaches to assessing sub-pixel classification results' accuracy [13]. Therefore, the mentioned accuracy assessments (Table 1) for the resulted SAM-based map were calculated using selected endmembers (Fig. 4) and relevant pixels (Training (198 pixels) and Testing (3788 pixels)).

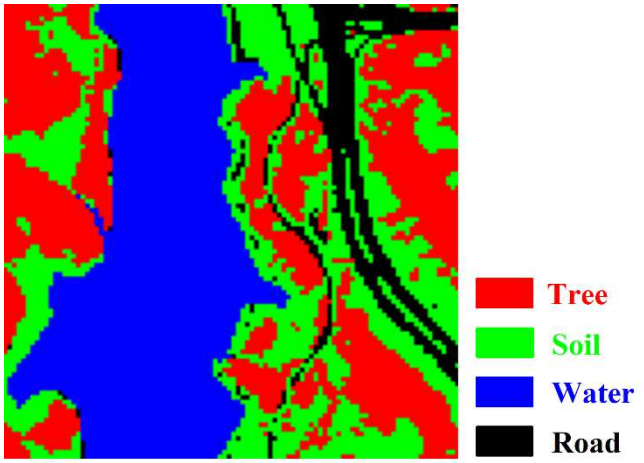

Fig. 5. Class map resulted from SAM method performed on LS unmixing.

In this study hence, conventional pixel-based accuracy evaluation methodology is adopted alternatively to assess the performance of the sub-pixel classification. The accuracies such as overall, producer's, users, and kappa statistics [20], [21], [22] were implemented, and these accuracies were evaluated using a confusion matrix. Table 1 indicates the evaluation of precision resulted from SAM classification. It was observed that the misclassification also has there between road and soil due to spectral similarity. The producer's accuracy for road and soil class is 97.54 and 92.12, and the user's accuracy is 77.61 and 83.62 percent, respectively. The producers' and user's accuracy for the tree and water class was satisfactory (Table 1). According to the results, it is noticed that the MNF transformation is essential to the LS spectral unmixing.

TABLE I. ACCURACY EVALUATION OF THE CLASSIFIED FEATURES RESULTED BY SAM METHOD

Classes	Producer's accuracy (%)	User's accuracy (%)	Overall accuracy (%)	Kappa statistics
Tree	97.84	97.68	94.19	0.90
Soil	92.12	83.62		
Water	93.20	100.00		
Road	97.54	77.61		

IV. CONCLUSIONS

Sub-pixel classification of hyperspectral images is efficient in applying spectral unmixing methods. The LS unmixing method helps classify the hyperspectral image by showing a 94.19% classification accuracy with 0.90 kappa statistics. The performance of the LS unmixing method has been increased when the image noise has been segregated using the MNF algorithm. Therefore, it is suggested that the LS unmixing method should be executed on the Eigen images only for better performance. Nevertheless, the mixed pixel challenge should be considered in the entire classification procedure, including training the data, classification, and assessment. The experimental results of this study may provide a valid baseline for the hyperspectral images unmixing.

ACKNOWLEDGMENT

The authors would like to acknowledge the Dr. Le Sun for providing the hyperspectral datasets to carry out this study.

REFERENCES

[1] Y. Wang, C. Pan, S. Xiang, and F. Zhu, "Robust hyperspectral unmixing with correntropy-based metric," IEEE Transactions on Image Processing, vol. 24, no. 11, pp. 4027–4040, 2015.

[2] Zhu, F. (2017). Hyperspectral unmixing: ground truth labeling, datasets, benchmark performances and survey. arXiv preprint arXiv:1708.05125.

[3] Zhou, L., Zhang, X., Wang, J., Bai, X., Tong, L., Zhang, L., ... & Hancock, E. (2020). Subspace structure regularized nonnegative matrix factorization for hyperspectral unmixing. IEEE Journal of Selected Topics in Applied Earth Observations and Remote Sensing, 13, 4257-4270.

[4] Guo, A. J., & Zhu, F. (2021). Improving deep hyperspectral image classification performance with spectral unmixing. Signal Processing, 183, 107949.

[5] Ahmed, A. M., Duran, O., Zweiri, Y., & Smith, M. (2017). Hybrid spectral unmixing: using artificial neural networks for linear/non-linear switching. Remote Sensing, 9(8), 775.

[6] Arun, P. V., Buddhiraju, K. M., & Porwal, A. (2018). CNN based sub-pixel mapping for hyperspectral images. Neurocomputing, 311, 51-64.

[7] Chen, S., Li, X., & Zhao, L. (2017). Subpixel mapping method of hyperspectral images based on modified binary quantum particle swarm optimization. Journal of Electrical and Computer Engineering, 2017.

[8] Guo, Z., Wittman, T., & Osher, S. (2009, April). L1 unmixing and its application to hyperspectral image enhancement. In Algorithms and Technologies for Multispectral, Hyperspectral, and Ultraspectral Imagery XV (Vol. 7334, p. 73341M). International Society for Optics and Photonics.

[9] Dong, W., Fu, F., Shi, G., Cao, X., Wu, J., Li, G., & Li, X. (2016). Hyperspectral image super-resolution via non-negative structured sparse representation. IEEE Transactions on Image Processing, 25(5), 2337-2352.

[10] Li, C., Sun, T., Kelly, K. F., & Zhang, Y. (2011). A compressive sensing and unmixing scheme for hyperspectral data processing. IEEE Transactions on Image Processing, 21(3), 1200-1210.

[11] Qian, Y., Jia, S., Zhou, J., & Robles-Kelly, A. (2011). Hyperspectral unmixing via $ L_ {1/2} $ sparsity-constrained nonnegative matrix factorization. IEEE Transactions on Geoscience and Remote Sensing, 49(11), 4282-4297.

[12] Ibarrola-Ulzurrun, E., Drumetz, L., Marcello, J., Gonzalo-Martin, C., & Chanussot, J. (2019). Hyperspectral classification through unmixing abundance maps addressing spectral variability. IEEE Transactions on Geoscience and Remote Sensing, 57(7), 4775-4788.

[13] Tseng, Y. H. (2000). Spectral unmixing for the classification of hyperspectral images. International Archives of Photogrammetry and Remote Sensing, 33(B7/4; PART 7), 1532-1538.

[14] Zhuo, R., Xu, L., Peng, J., & Chen, Y. (2018). Spectral Unmixing Analysis of Time Series Landsat 8 Images. International Archives of the Photogrammetry, Remote Sensing and Spatial Information Sciences, 42, 3.

[15] http://lesun.weebly.com/hyperspectral-data-set.html.

[16] Vibhute, A. D., Kale, K. V., Dhumal, R. K., & Mehrotra, S. C. (2015, December). Hyperspectral imaging data atmospheric correction challenges and solutions using QUAC and FLAASH algorithms. In 2015 International Conference on Man and Machine Interfacing (MAMI) (pp. 1-6). IEEE.

[17] Zeng, Y., Ritz, C., Zhao, J., & Lan, J. (2019). Scattering transform framework for unmixing of hyperspectral data. Remote Sensing, 11(23), 2868.

[18] Vibhute, A. D., Kale, K. V., Dhumal, R. K., Nagne, A. D., Mehrotra, S. C., Varpe, A. B., Surase, R. R, Nalawade, D. B. & Gaikwad, S. V. (2019). Spectral Feature Extraction and Classification of Soil Types Using EO-1 Hyperion and Field Spectroradiometer Data Based on PCA and SVM. In Microelectronics, Electromagnetics and Telecommunications (pp. 525-533). Springer, Singapore.

[19] Luo, G., Chen, G., Tian, L., Qin, K., & Qian, S. E. (2016). Minimum noise fraction versus principal component analysis as a preprocessing step for hyperspectral imagery denoising. Canadian Journal of Remote Sensing, 42(2), 106-116.

[20] Vibhute, A. D., Kale, K. V., Gaikwad, S. V., Dhumal, R. K., Nagne, A. D., Varpe, A. B., Nalawade, D. B. & Mehrotra, S. C. (2020). Classification of complex environments using pixel level fusion of satellite data. Multimedia Tools and Applications, 79, 34737-34769.

[21] Vibhute, A. D., Kale, K. V., Dhumal, R. K., Nagne, A. D., & Mehrotra, S. C. (2018). Identification, Classification and Mapping of Surface Soil Types using Hyperspetral Remote Sensing Datasets. International Journal of Scientific Research in Computer Science, Engineering and Information Technology, 3(1), 921-932.

[22] Vibhute, A. D., Dhumal, R. K., Nagne, A. D., Rajendra, Y. D., Kale, K. V., & Mehrotra, S. C. (2016). Analysis, classification, and estimation of pattern for land of Aurangabad region using high-resolution satellite image. In Proceedings of the Second International Conference on Computer and Communication Technologies (pp. 413-427). Springer, New Delhi.